2268 *Chem. Mater.* **2010,** *22,* 2268–2275
DOI:10.1021/cm902898k

CHEMISTRY OF MATERIALS
Article

Electron Paramagnetic Resonance, X-ray Diffraction, Mössbauer Spectroscopy, and Electrochemical Studies on Nanocrystalline $FeSn_2$ Obtained by Reduction of Salts in Tetraethylene Glycol

Uche G. Nwokeke,[†] Ricardo Alcántara,[†] José L. Tirado,*[,†] Radostina Stoyanova,[‡] Meglena Yoncheva,[‡] and Ekaterina Zhecheva[‡]

[†]*Laboratorio de Química Inorgánica. Universidad de Córdoba Edificio C3, Campus de Rabanales 14071 Córdoba, Spain, and* [‡]*Institute of General and Inorganic Chemistry Bulgarian Academy of Sciences 1113 Sofia, Bulgaria*

Received September 17, 2009. Revised Manuscript Received February 16, 2010

Nanocrystalline $FeSn_2$ was prepared by chemical reduction of Sn−Fe chlorides in tetraethylene glycol using a "one-pot" method. Structural characterization is carried out by powder X-ray diffraction (XRD), transmission electron microscopy (TEM), and ^{119}Sn Mössbauer spectroscopy. The electrochemical reaction of nanocrystalline $FeSn_2$ with Li was examined by electron paramagnetic resonance (EPR) and ^{57}Fe Mössbauer spectroscopy. Nanocrystalline $FeSn_2$ delivers reversible capacities of about 600 $mAhg^{-1}$ vs lithium after 20 cycles. The mechanism of the electrochemical reaction involves the conversion of $FeSn_2$ into Li_xSn phases and superparamagnetic iron (or tin-doped iron) nanoparticles. The composition and the dimensions of the superparamagnetic particles depend on the depth of discharge. The electrochemically formed superparamagnetic particles are preserved in the course of the reverse electrochemical reaction.

Introduction

The finding of novel electrode materials for high-power and high-density lithium ion batteries is one of the most widely investigated topics in materials chemistry in the last few decades.[1−6] To this aim, several systems such as lithium transition metal oxides, carbonaceous materials, and alloys have been employed. Among them, lithium alloys and intermetallics attracted the research interest early due to their high theoretical capacity.[7,8] Recent research in the field evidence that tin and tin compounds are a hot topic in the present state-of the art of electrode materials for lithium-ion batteries.[9−13] The application of advanced spectroscopic techniques has proven to be particularly helpful to shed new light on the mechanism of the electrochemical reactions with lithium and to envisage new ways to improve the performance of the electrode materials.[11,14−21]

Elemental tin exhibits the capability to alloy with lithium and might be used as the negative electrode in lithium ion batteries. The maximum theoretical capacity for the Li−Sn system is 990 $mAhg^{-1}$. This capacity value corresponds to the formation of the intermetallic compound $Li_{22}Sn_5$ (788 $mAhg^{-1}$ for Li_7Sn_2).[8,14] However, pure tin electrodes usually exhibit abrupt volume changes, decrepitation, and consequently capacity fade upon electrochemical cycling. The incorporation of electrochemically inactive elements would decrease the maximum theoretical capacity of pure tin, but a net gain of stability upon cycling can be achieved. Thus, the addition of 3d elements, such as iron, cobalt, and nickel, seems to be especially advantageous. Because of the low cost and low toxicity, the use of iron is particularly interesting, and several studies have been published on the Fe−Sn system.

(1) Whittingham, M. *Science* **1976**, *192*, 1226.
(2) Winter, M.; Besenhard, J. O.; Spahr, M. E.; Novak, P. *Adv. Mater.* **1998**, *10*, 725.
(3) Tarascon, J.-M.; Armand, M. *Nature* **2001**, *414*, 359.
(4) Tirado, J. L. *Mater. Sci. Eng.* **2003**, *40*, 103.
(5) Whittingham, M. S. *Chem. Rev.* **2004**, *104*, 4271.
(6) Arico, A. S.; Bruce, P.; Scrosati, B.; Tarascon, J.-M.; van Schalkwijk, W. *Nat. Mater.* **2005**, *4*, 366.
(7) Besenhard, J. O.; Yang, J.; Winter, M. *J. Power Sources* **1997**, *68*, 87.
(8) Dunlap, R. A.; Small, R. A.; McNeil, D. D.; Obrovac, M. N.; Dahn, J. R. *J. Alloys Compd.* **1999**, *289*, 135.
(9) Hassoun, J.; Reale, P.; Scrosati, B. *J. Mater. Chem.* **2007**, *17*, 3668.
(10) Lou, X. W.; Deng, D.; Lee, J. Y.; Archer, L. A. *Chem. Mater.* **2008**, *20*, 6562.
(11) Ehinon, K. K. D.; Naille, S.; Dedryvère, R.; Lippens, P.-E.; Jumas, J.-C.; Gonbeau, D. *Chem. Mater.* **2008**, *20*, 5388.
(12) Wang, Y.; Wu, M.; Jiao, Z.; Lee, J. Y. *Chem. Mater.* **2009**, *21*, 3210.
(13) Wang, Y.; Djerdj, I.; Smarsly, B.; Antonietti, M. *Chem. Mater.* **2009**, *21*, 3202.
(14) Naille, S.; Dedryvère, R.; Zitoun, D.; Lippens, P. E. *J. Power Sources* **2009**, *189*, 806.
(15) Mao, O.; Dunlap, R. D.; Dahn, J. R. *J. Electrochem. Soc.* **1999**, *146*, 405.
(16) Mao, O.; Dunlap, R. A.; Courtney, I. A.; Dahn, J. R. *J. Electrochem. Soc.* **1998**, *145*, 4195.
(17) Mao, O.; Dahn, J. R. *J. Electrochem. Soc.* **1999**, *146*, 414.
(18) Mao, O.; Turner, R. L.; Courtney, I. A.; Fredericksen, B. D.; Buckett, M. I.; Krause, L. J.; Dahn, J. R. *Electrochem. Solid State Lett.* **1999**, *2*, 3.
(19) Ferguson, P. P.; Liao, P.; Dunlap, R. A.; Dahn, J. R. *J. Electrochem. Soc.* **2009**, *156*, A13.
(20) Zhang, C. Q.; Tu, J. P.; Huang, X. H.; Yuan, Y. F.; Wang, S. F.; Mao, F. *J. Alloys Compd.* **2008**, *457*, 81.
(21) Mao, O.; Dunlap, R. A.; Dahn, J. R. *Solid State Ionics* **1999**, *118*, 99.

Published on Web 02/25/2010

The $FeSn_2$ compound could yield a maximum capacity of 802 $mAhg^{-1}$ according to the next reaction process:[15]

$$44Li + 5FeSn_2 \rightleftarrows 2Li_{22}Sn_5 + 5Fe \quad (1)$$

Mao et al. studied the electrochemical behavior of $FeSn_2$ obtained by arc melting followed by mechanical alloying.[16] Several other $FeSn_x$ phases with higher iron content, such as FeSn, Fe_3Sn_2, and Fe_5Sn_3, tend to form an electrochemically inactive "skin" of Fe over the surface of the active particles that prevents the full reaction with lithium.[17] In order to improve the electrochemical behavior, a composite electrode obtained by ball-milling of Fe, Sn, and C was also reported.[18] Having in mind that $CoSn_2$ and $FeSn_2$ are isostructural and the use of iron can be economically and environmentally advantageous, recently, $FeSn_2$ has been used to obtain nanostructured Sn−Co−Fe−C composite materials throughout mechanical alloying.[19] However, iron-containing intermetallics used to show poor capacity retention upon electrochemical cycling. In general, one may expect to improve the electrochemical performance of $FeSn_x$-based anodes by using nanoscale materials,[20] since they are able to accommodate lattice strains more easily, to increase the contacts between the inactive "skin" and the Li_xSn-particles and to change the reaction mechanism. Zhang et al. reported that nanoscale $FeSn_2$ (prepared by the chemical reduction process and by the solvothermal method) delivered a reversible discharge capacity of about 500 mAh/g.[20]

The improvement of the electrode materials requires an in-depth knowledge of the mechanism of the reactions with lithium. The mechanism of interaction of $FeSn_x$ intermetallics with Li has been previously studied by means of X-ray diffraction (XRD) and ^{119}Sn and ^{57}Fe Mössbauer spectroscopy.[17,21] Another spectroscopic method that is suitable for structural characterization of iron metal and iron oxides as bulk- and nanoparticles is the electron paramagnetic resonance spectroscopy (EPR).[22,23] This technique will allow going deeper into the mechanism of the electrochemical reaction of $FeSn_x$ with Li being that it is a sensitive and selective method.

With the study of nanostructured intermellics for lithium ion batteries in mind, in this work nanocrystalline $FeSn_2$ has been prepared by chemical reduction of salts in tetraethylene glycol using a "one-pot" method. Structural characterization is carried out by powder XRD, transmission electron microscopy (TEM), and ^{119}Sn Mössbauer spectroscopy. To study the electrochemical reaction of $FeSn_2$ with Li, EPR spectroscopy is used here for the first time.

Experimental Section

Nanocrystalline particles of $FeSn_2$ were obtained by following a method previously described.[24] This is a "one-pot" method which involves the sequential $NaBH_4$ reduction of the metal salts in tetraethylene glycol (TEG), followed by heating under argon-flow in the presence of poly(vinyl pyrrolidone) (PVP; MW = 40 000) and poly(2-ethyl-2-oxazoline) (PEO; MW = 50 000). The reagents were supplied by Aldrich. In this synthesis, 0.7 g of PVP and 0.3 g of PEO were dissolved in 45 mL of TEG. The solution was heated to 170 °C, and then $SnCl_2$ (0.130 g in 4 mL of TEG) was added. A solution of $NaBH_4$ (0.264 g in 8 mL of TEG) was then slowly added while stirring. After 12−15 min at 170 °C, $FeCl_3 \cdot 6H_2O$ (0.090 g in 4 mL of TEG) was added. The resulting solution was heated to 185 °C during 90 min, resulting in a black colloidal suspension. The $FeSn_2$ nanocrystals were separated by centrifugation, washed with ethanol, and finally dried under vacuum at 80 °C overnight.

The XRD patterns were obtained in a Siemens-D5000 instrument with CuKα radiation. TEM images were recorded by using a JEM-2010 apparatus.

^{119}Sn and ^{57}Fe Mössbauer spectra were recorded in transmission mode at room temperature by using a Wissel instrument. $Ba^{119}SnO_3$ and ^{57}Co in a Rh matrix were used as radioactive sources, respectively. The ^{119}Sn isomer shifts were referenced to $BaSnO_3$, and pure β-Sn foils were used for the instrument calibration. A pure α-Fe foil was used for calibration and as reference in the ^{57}Fe Mössbauer spectra. For the fitting of the experimental spectra, Lorentzian profiles and a least-squares method were employed. The fit quality was controlled by the χ^2-test. For Mössbauer measurements, used electrodes were kept inside a thermosealed bag (Aldrich) inside the drybox, and the bag was directly transferred to the Mössbauer system.

EPR spectra were registered at X-band (9.23 GHz) as the first derivative of the absorption signal using a ERS 220/Q spectrometer in the temperature range 90−410 K. The *g*-factors were established with respect to a Mn^{2+}/ZnS standard. The signal intensity was determined by double integration of the experimental EPR spectrum. For EPR measurements of anode materials, the samples were manipulated in a glovebox. All EPR measurements on dry electrode compositions (without electrolyte) were carried out in quartz tubes in an Ar atmosphere.

The electrochemical experiments were performed in an Arbin system and used lithium test cells. The electrolyte was $LiPF_6$ dissolved in an ethylene carbonate/diethyl carbonate mixture. Besides the active material ($FeSn_2$), the electrodes were constituted by graphite and polyvinylidene fluoride (PVDF). The relative amounts were active material (87%), graphite (8%), and PVDF (5%) or, alternatively, active material (77%), graphite (15%), and PVDF (8%). The used currents were between 30 and 240 mA/g. In order to prepare electrodes for ex situ measurements close to equilibrium, lower intensities were imposed.

Results and Discussion

Structure Characterization. The observed XRD pattern of the obtained $FeSn_2$ sample (Figure 1) agrees well with the diffraction file number 25-415. Crystalline impurities are not observed. The calculated tetragonal lattice cells parameters are $a = b = 6.55(1)$ Å and $c = 5.365(2)$ Å. The average grain size obtained by applying the Scherrer equation to the most intense reflection is equal to 26 nm. The TEM micrographs (Figure 2) show nanometric particles with poorly defined morphologies. The observation of lattice fringes within small domains evidence the nanocrystalline character of the sample. Particle size was not uniform but varied in the 6−30 nm range (Figure 2,

(22) Alcántara, R.; Lavela, P.; Ortiz, G. F.; Tirado, J. L.; Stoyanova, R.; Zhecheva, E.; Jiménez-Mateos, J. M. *J. Electrochem. Soc.* **2004**, *151*, A2113.
(23) Lavela, P.; Ortiz, G.; Tirado, J. L.; Zhecheva, E.; Stoyanova, R.; Ivanova, Sv. *J. Phys. Chem. C* **2007**, *111*, 14238.
(24) Cable, R. E.; Schaak, R. E. *Chem. Mater.* **2005**, *17*, 6835.

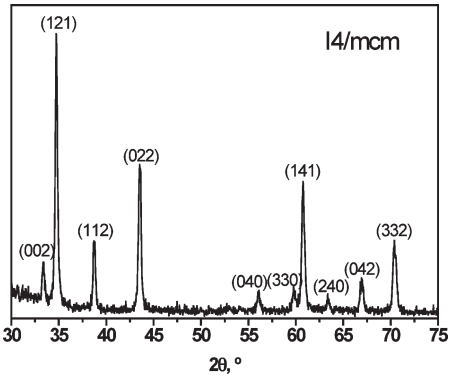

Figure 1. XRD pattern for $FeSn_2$. The Miller indexes are indicated.

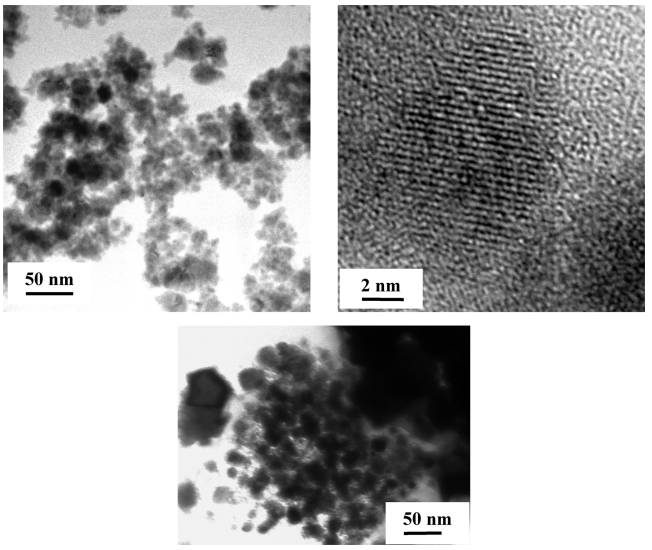

Figure 2. Upper: TEM micrographs for $FeSn_2$. Lower: micrograph of used electrode after the first charge.

left), leading to an average value close to the Scherrer crystallite size.

The room temperature ^{119}Sn Mössbauer spectrum of nanocrystalline $FeSn_2$ shows a broadened and low-intensity signal that can be fitted with a doublet (Figure 3, Table 1). This doublet is centered at isomer shift δ = 1.91(3) mm/s and the quadrupole splitting value is Δ = 2.10(4) mm/s. The bonding with some covalent character reduces the electron densities at the nuclei and decreases the isomer shift value as compared to pure Sn.[25] Tin oxides are not detected. The small particle size can decrease the recoil-free fraction of the tin atoms and decrease the signal intensity.

According to previous neutron diffraction and Mössbauer spectroscopy studies,[26] micrometric $FeSn_2$ is antiferromagnetic below 378 K (T_N), and a second magnetic transition occurs at 93 K (T_t). Between T_N and T_t, the magnetic structure is collinear and characterized by ferromagnetic (100) planes, antiferromagnetically coupled along the [100] direction. Below T_t, $FeSn_2$ becomes

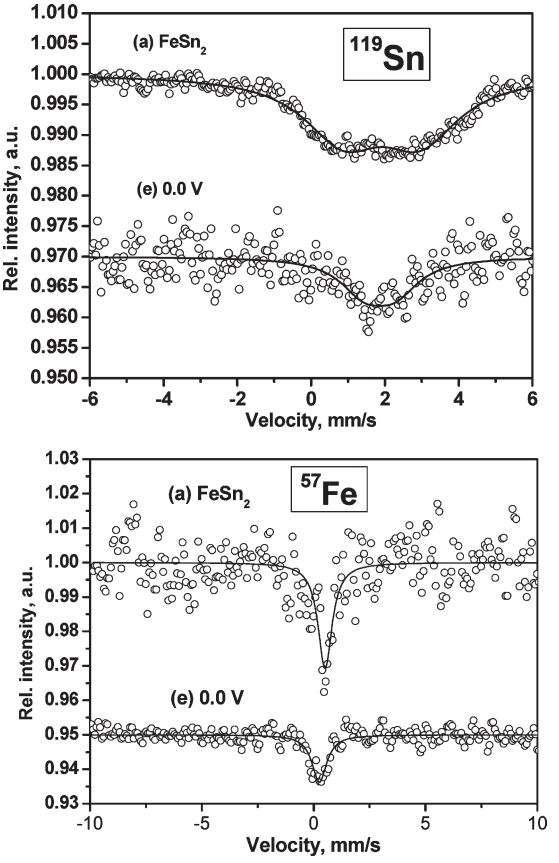

Figure 3. ^{119}Sn and ^{57}Fe Mössbauer spectra of pristine nanocrystalline $FeSn_2$ and electrodes discharged to 0.0 V.

Table 1. Results of the ^{119}Sn and ^{57}Fe Mössbauer Spectra Fitting for $FeSn_2$ Electrodes[a]

notation	atom	δ	Δ	Γ	C
(a) pristine	^{119}Sn	1.92(3)	2.09(4)	2.6(1)	100
	^{57}Fe	0.51(4)		0.8(1)	100
(e) 0.0 V	^{119}Sn	1.9(1)	0.8(2)	1.6(4)	100
	^{57}Fe	0.26(3)		0.8(1)	100

[a] See the meaning of the notation by following Figure 7. δ, isomer shift (mm s^{-1}); Δ, quadrupole splitting (mm s^{-1}); Γ, line width (mm s^{-1}); C, relative contribution (%).

noncollinear antiferromagnetic. For $FeSn_2$ with very small grain sizes, a superparamagnetic state is found at room temperature.[15] The ^{57}Fe Mössbauer spectra of the initial sample (Figure 3, bottom) agrees with this description. A superparamagnetic singlet is observed with the expected isomer shift (0.51(4) mm/s, Table 1) for the intermetallic compound.[15,19]

EPR was furthermore used for analysis of nanocrystalline $FeSn_2$. The influence of the small particle sizes is evidenced on the EPR spectra. At high-registration temperature, the EPR spectrum of pristine nanosized $FeSn_2$ consists of a nearly symmetric line (Figure 4). The EPR signal becomes anisotropic upon cooling. In the same time, the EPR signal intensity decreases; and below 140 K, the signal disappears. This means that for pristine nanosized $FeSn_2$, the EPR signal comes from magnetically correlated spins, which are ordered in a long-range below 140 K. The EPR results are in agreement with the magnetic

(25) Trumpy, G.; Both, E.; Djega-Mariadassou, C. *Phys. Rev. B* **1970**, *2*, 3477.
(26) Wodniecka, B.; Wodniecki, P.; Kulinska, A.; Hrynkiewicz, A. Z. *J. Alloys Compd.* **2001**, *321*, 1.

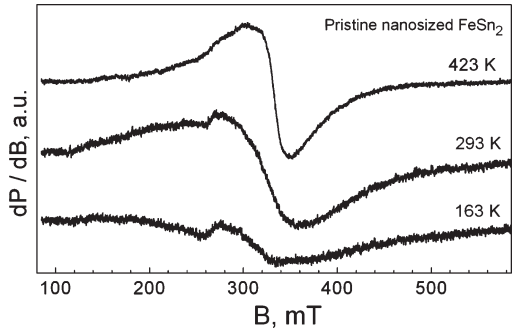

Figure 4. EPR spectra of pristine $FeSn_2$ at several temperatures.

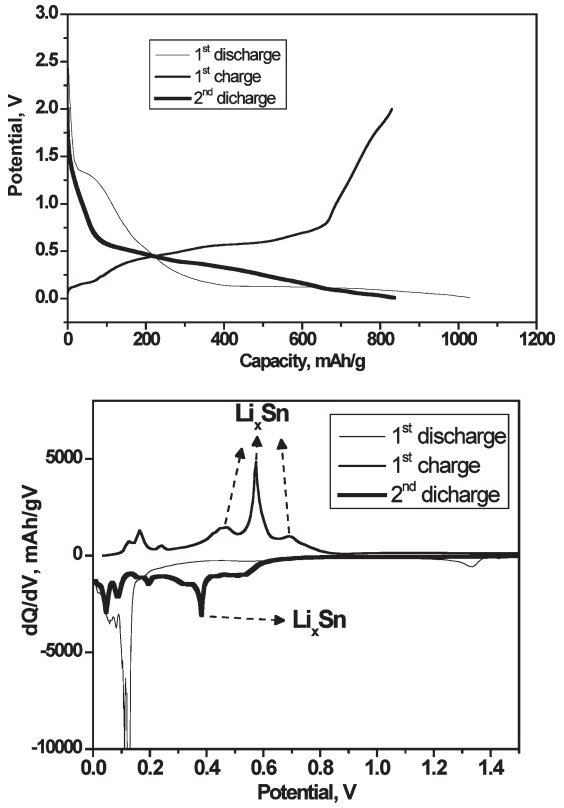

Figure 5. Potential−capacity plot and the corresponding derivative curves.

properties of nanocrystalline Fe−Sn alloys.[27,15] On the basis of magnetic susceptibility measurements, it has been found that the temperature of long-range magnetic order of $FeSn_2$ is 140 K.[27] It is worth mentioning that there is no presence of resonance signal due to iron oxide phases. This result outlines the capability of the "one-pot" method to prepare pure $FeSn_2$.

Electrochemistry. The electrochemical behavior of nanocrystalline $FeSn_2$ in lithium test cells is shown in Figures 5 and 6. The capacity of the first discharge, which is referenced to the mass of $FeSn_2$, exceeds the theoretical maximum value (Figure 5). Henceforth, it is assumable that side reactions are taking place in the surface of the nanoparticles. The graphite additive used as a conductive agent also can contribute to the excess of capacity. The irreversible part of

(27) Yelsukov, E. P.; Konygin, G. N.; Voronina, E. V.; Korolyov, A. V.; Ulyanov, A. I.; Godovikov, S. K.; Zagainov, A. V. *J. Magn. Magn. Mater.* **2000**, *214*, 258.

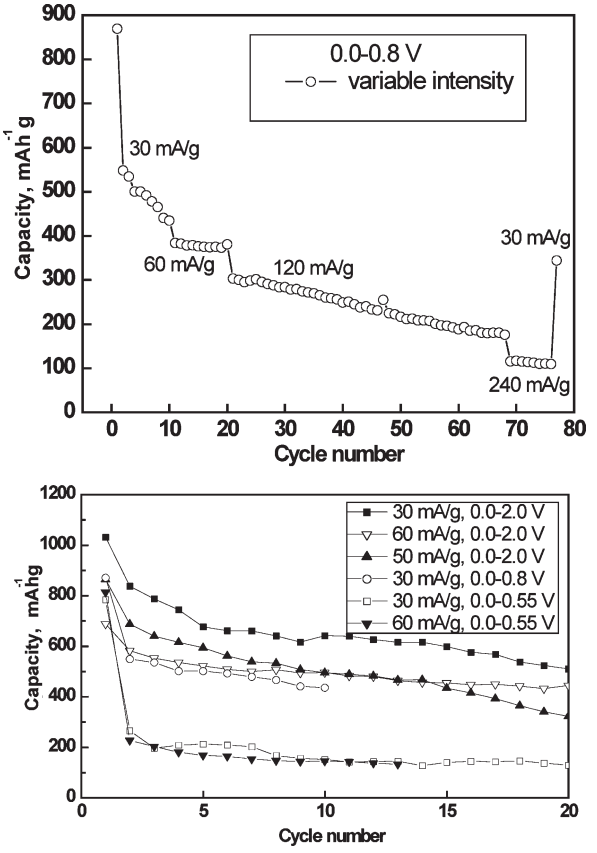

Figure 6. Specific capacity as a function of cycle number at several current intensities and potential limits.

the first cycle is around 200 mAh/g, depending on the cycling conditions. Reversible capacities values slightly over 800 mAh/g are observed in the first cycles. The values are near the maximum theoretical capacity (802 mAh/g). Most of this capacity is delivered between 0.0 and 0.8 V.

The derivative curve of the first discharge exhibits a very intense peak at ~0.1 V and a low-intensity signal at 1.3 V (Figure 5). The peak at 1.3 V is irreversible and ascribable to side reactions such as electrolyte solution consumption and formation of a solid electrolyte interface or, alternatively, to true lithium insertion into $FeSn_2$. In addition, the participation of some organic residues (such as PEO and TEG) in side reactions can not be ruled out. The peak at 0.1 V is also irreversible and is ascribed to the destruction of the $FeSn_2$ structure and formation of lithium-containing intermetallics. The formation of Fe and Li_xSn grains was previously reported.[15] In the charge process, the peaks centered at 0.57, 0.45, and 0.7 V are ascribed to the extraction of lithium from Li_xSn phases. The peak centered at 0.38 V in the second discharge is ascribed to the formation of Li_xSn. The iron atoms seem to act as "spectators" in the electrochemical reactions between Li and Sn and might help to maintain the electrode integrity. These results are in agreement with previous studies.[16]

For 2.0 and 0.8 V as upper potential limits, the observed capacity retention is poor, independent of the current (Figure 6). It seems that the volume changes due to Li−Sn alloying and dealloying processes lead to the loss of electrical

contact between the particles. The capacity decreases when the current is increased from 30 to 240 mA/g. An enhanced cycle life for the cells cycled between 0 and 0.55 V was observed by other authors.[15] The performances of the nanomaterials described here compare well with other recently described systems, with more than 500 mAh/g after 20 cycles for low rates and more than 400 at a higher rate. The performance of these nanodispersed materials is significantly improved as compared with bulk samples (see, for example, ref 16 for mechanically alloyed $FeSn_2$).

Reaction Mechanism. To study the reaction mechanism, the electrochemical cells were interrupted at selected states of discharge−charge, and XRD (Figure 7) and spectroscopic measurements were carried out ex situ. In addition, TEM of used electrodes showed that nanosized particles are still present, so that the superparamagnetic character of the nanodomains could be preserved (Figure 2, lower). However, this possibility will be discussed below in the light of the EPR results.

After partial discharge to 495 mAh/g, the XRD pattern (Figure 7d) still exhibits the reflections of the $FeSn_2$ phase, and the reaction products remain XRD-undetectable. Mao et al. observed residual $FeSn_2$ after whole discharge, and this phase disappeared after holding the cell at 0 V for 1 day.[15] After partial discharge to 600 mAh/g and recharge up to 2.0 V (Figure 7g), low-intensity reflections corresponding to unreacted $FeSn_2$ are observed, and a narrow reflection corresponding to $Li_{13}Sn_5$ (ICDD file no. 29-0838) is also observed. After complete discharge to 0.0 V (Figure 7e), the original $FeSn_2$ is not detected, while the low-intensity reflections observed at ~24 and 39°/2θ are ambiguously ascribable to both $Li_{22}Sn_5$[8] and Li_7Sn_2.[14] Metallic iron is not detected. These features imply the segregation of iron (XRD-undetected small grains) from the original $FeSn_2$ phase and formation of Li_xSn phases (see eq 1). For that reason, ex situ Mössbauer spectroscopy was used to complement XRD experiments. Irrespective of the low absorption, the ^{119}Sn Mössbauer spectrum of the discharged electrode (0.0 V, Figure 3, Table 1) becomes narrower than the starting $FeSn_2$ spectrum and is centered at a value (δ = 1.9(1) mm/s) that is close to the values corresponding to $Li_{22}Sn_5$ (δ = 1.837(3) mm/s) or Li_7Sn_2 (average shift 1.960 mm/s).

The ^{57}Fe Mössbauer spectra of the initial sample (Figure 3, Table 1) shows that the isomer shift decreases significantly after lithium insertion, which is indicative of the conversion from $FeSn_2$ to metallic iron. However, the shift never reaches 0.0 mm/s, the value corresponding to α-Fe. Also the magnetic ordering of α-Fe is not seen at room temperature, probably indicating the superparamagnetic nature of the iron product, most probably in the form of nanodomains. In addition, it has been shown that small amount of tin can be incorporated into α-Fe leading to the formation of α-$Fe_{1-x}Sn_x$ with $x \leq 0.08$.[28] The possible contribution of tin containing iron superparamagnetic particles on the ^{57}Fe Mössbauer spectrum can also be taken into account. The EPR data described below shed new light on these phenomena.

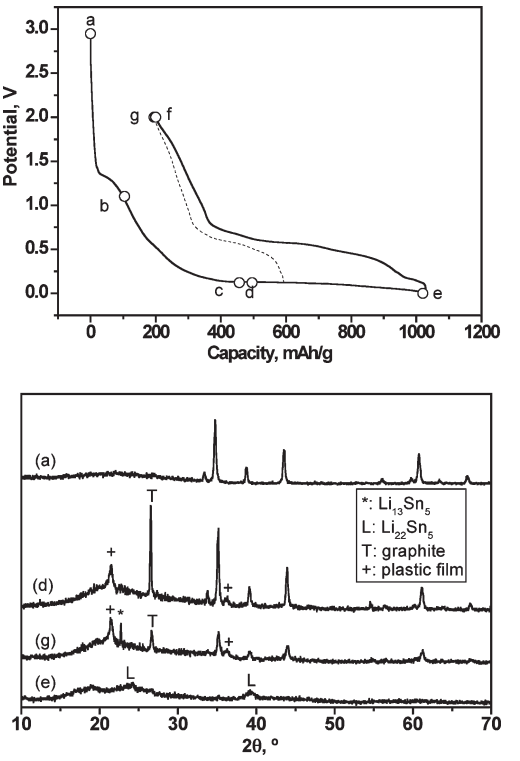

Figure 7. (Top) The selected points for ex situ measurements are indicated (a−g). (Bottom) XRD patterns for pristine $FeSn_2$ (a) and recuperated electrodes at selected states of discharge (d, e) and recharge (g).

The EPR spectrum of $FeSn_2$ is changed immediately after a lower depth of discharge (Figure 8b). In the temperature range of 100−300 K, the EPR spectrum displays a single line with Lorentzian shape. The Lorentzian signal is broadened on cooling together with a shift of the effective resonance absorption toward a lower magnetic field (Figure 8). For $FeSn_2$ with a higher depth of discharge, the Lorentzian line shape is preserved. The effective *g*-factor and the EPR line width depend on the registration temperature in the same manner as in the case of $FeSn_2$ with a lower depth of discharge (Figure 8c,d). This means that EPR signal has the same origin for samples with different discharge depth. The observed EPR parameters are typical for superparamagnetic resonance (SPR). For randomly oriented monodomain magnetic particles, a phenomenological description of the relationship between the line width and the shift of the effective resonance absorption has been proposed by Nagata and Ishimira:[29] $(B_r - B_{r(T=293)}) \sim \Delta H_{pp}{}^3$, where $(B_r - B_{r(HT)})$ corresponds to the resonance field shift in respect of the resonance at high temperature and ΔH_{pp} is the line width. Figure 9 gives this relationship for $FeSn_2$ partially discharged (parts b−d) and totally discharged (e). As one can see, the relationship is obeyed for the three electrodes. This relation evidences the presence of a single domain superparamagnetic phase, which corroborates ^{57}Fe Mössbauer studies of discharged $FeSn_2$ electrodes.

(28) Berger, R.; Bissey, J.-C.; Kliava, J. *J. Phys.: Condens. Matter* **2000**, *12*, 9347.

(29) Giefers, H.; Nicol, M. *J. Alloys Compd.* **2006**, *422*, 132.

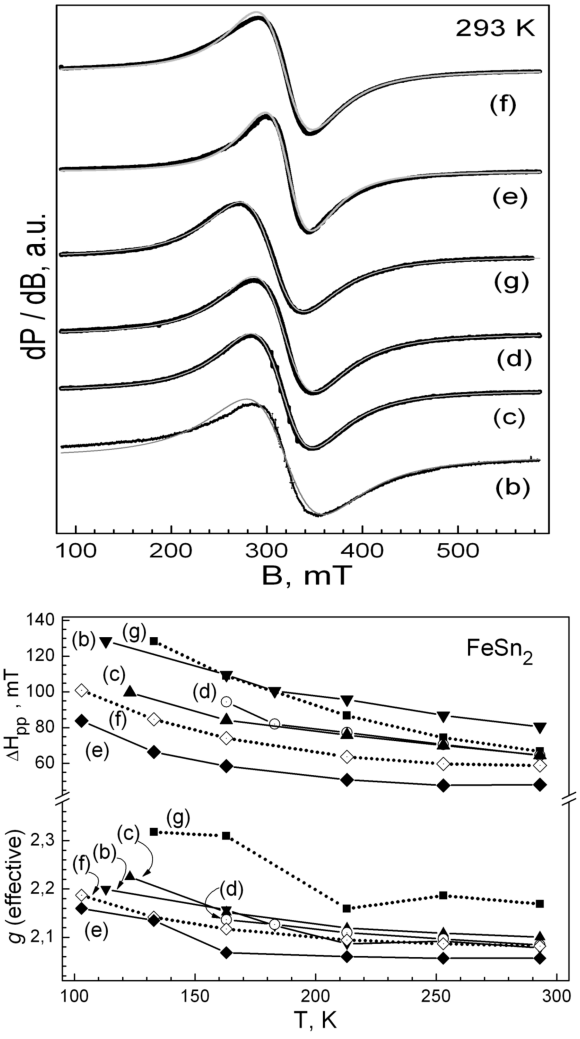

Figure 8. (Top) EPR spectra of $FeSn_2$ electrodes at selected states of discharge (b−e) and recharge (g,f). (Bottom) Effective *g*-factor and EPR line width, ΔH_{pp}, of $FeSn_2$ electrodes.

The EPR parameters that change with the depth of discharge are the line width and the signal intensity (Figure 10). There is a smooth decrease in the line width with the discharge depth. The signal intensity increases dramatically, passing through a maximum at a discharge depth of 460 mAh/g (Figure 10). It should be mentioned that for superparamagnetic resonance, the signal intensity follows the particle magnetization which in turn is determined by the particle shape and dimension.[29,30] This means that the variation in the signal intensity can be related with the temperature dependence of magnetization of the superparamagnetic particles.[31] For samples with a lower depth of discharge, the signal intensity is reversibly proportional to the registration temperature in accordance with Curie law (Figure 11). The slope of the "$I-1/T$" dependence is controlled by the spontaneous magnetization and the volume of the particles. This behavior is characteristic of a superparamagnetic assembly of

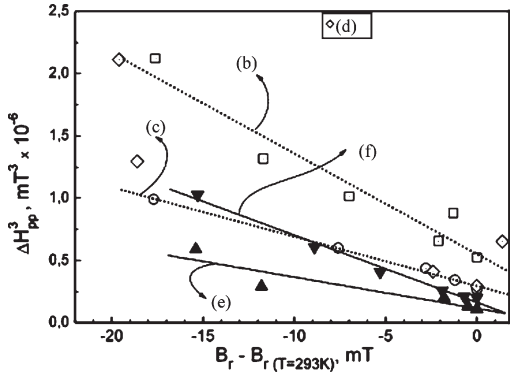

Figure 9. Relationship between the resonance field shift (relative to a higher-temperature value, $(B_r - B_{r(T)293)})$ and line width, ΔH_{pp}^3.

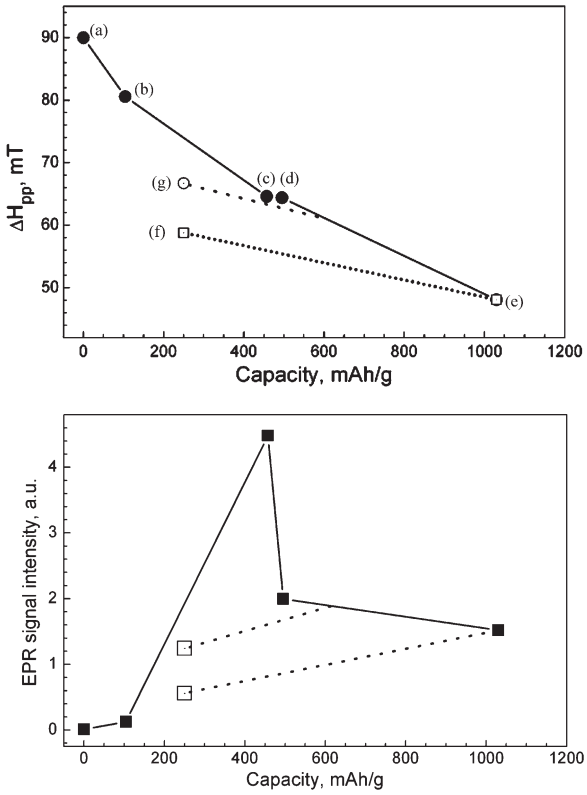

Figure 10. EPR line width (ΔH_{pp}) and signal intensity versus depth of discharge of $FeSn_2$. The open symbol corresponds to recharged samples.

ferromagnetic nanoparticles with close size distribution. When the depth of discharge increases, the temperature dependence of the signal intensity becomes more complex. This indicates an appearance of superparamagnetic particles with different magnetizations and volumes.

When $FeSn_2$ is recharged to 2 V, the EPR spectrum of pristine $FeSn_2$ is not recovered (Figure 8f). The EPR spectrum consists of a narrow Lorentzian line with EPR parameters close to that of discharged $FeSn_2$. This indicates that signal from superparamagnetic particles contributes also to the EPR spectrum of recharged $FeSn_2$. It is noticeable that the signal intensity is lower as compared to discharged samples (Figure 10). In addition, the EPR line width and signal intensity of recharged $FeSn_2$ depend on the depth of the first discharge. When $FeSn_2$ is discharged to 600 mAh/g followed by a charge to 2.0 V (part g),

(30) Nagata, K.; Ishihara, A. *J. Magn. Magn. Mater.* **1992**, *1571*, 104.
(31) Respaud, M.; Broto, J. M.; Rakoto, H.; Fert, A. R.; Thomas, L.; Barbara, B.; Verelst, M.; Snoeck, E.; Lecante, P.; Mosset, A.; Osuna, J.; Ould Ely, T.; Amiens, C.; Chaudret, B. *Phys. Rev. B* **1998**, *57*, 2925–2935.

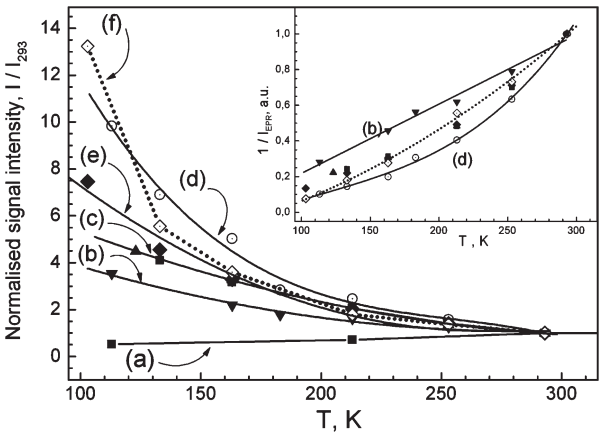

Figure 11. Temperature dependence of the signal intensity of pristine $FeSn_2$ and $FeSn_2$ electrodes at selected states of discharge (b−e) and recharge (g,f).

the EPR line width and signal intensity are higher in comparison to that of $FeSn_2$ discharged to 1030 mAh/g and subsequently charged to 2.0 V (part f). Contrary to deeply discharged electrodes, the temperature dependence of the signal intensity falls on a straight line (Figure 11). This indicates a change in magnetization and volume of superparamagnetic particles. To describe the picture quantitatively, EPR standards for superparamagnetic Fe and Sn-doped Fe are needed. The lack of suitable EPR standards prevents the accurate theoretical calculations of EPR spectra.

To assign the superparamagnetic resonance signal, the ^{57}Fe Mössbauer data on the decomposition of $FeSn_2$ during the electrochemical reaction are taken into account. Thus, we can attribute the EPR signal to iron particles in a superparamagnetic state. In addition, metal iron is able to accommodate small amounts of tin with preservation of its crystal structure.[28] Both α-Fe and Sn doped α-Fe are in ferromagnetic states. The average magnetic moment per Fe atom slightly increases from 2.22 to 2.3 μ_B after an increase in Sn content from 0 to 5 atom % Sn and remains nearly constant between 5 and 25 atom % Sn.[32] This means that tin-containing iron particles in a superparamagnetic state can also give rise to the superparamagnetic resonance signal of the charged and discharged electrodes. From an EPR point of view, the differentiation between superparamagnetic iron and superparamagnetic tin-containing iron particles is a difficult task. Irrespective of the composition of the superparamagnetic particles, the relationship between the line width and the particle size has been established experimentally: the line width decreases with decreasing the particle size.[33] This dependence is valid only in the case when interparticle magnetic interactions are absent. Hence, the important finding of EPR is the formation of superparamagnetic particles containing iron (or tin−iron) during the electrochemical reaction.

The changes in the EPR line width and the signal intensity with the discharge depth can be related with the variation of both the composition and the dimensions of the superparamagnetic particles. It is noticeable that nanoparticles with a narrow size distribution start to form at the beginning of the discharge, where the solid−electrolyte interface is developed, and most of $FeSn_2$ remains unreacted (Figures 5 and 7). This means that, at lower depth of discharge, the formation of superparamagnetic particles proceeds mainly on the particle surface. The signal intensity increases with the discharge depth, reaching a maximum at 457 mAh/g. For deeply discharged electrodes where Li_xSn phases are formed, a "loss" of signal intensity is observed and the size distribution becomes broader. This fact can be understood if we take into account that the amount of the tin impurities will affect the EPR response from the iron superparamagnetic particles. In addition, the EPR spectroscopy is sensitive towards the dimensions of the superparamagnetic particles.[21] This means that in the course of the electrochemical reaction, a redistribution of the superparamagnetic particles takes place leading to a particle growth and a loss in the EPR intensity. It is noticeable that the formation of an electrochemically inactive "skin" of Fe on the surface of FeSn particles during the charge process has been established by ^{57}Fe and ^{119}Sn Mossbauer spectroscopy.[17]

After the first discharge, the electrochemical reaction proceeds with the participation of Li_xSn phases. Similarly, iron superparamagnetic particles are preserved. However, the small variation in the EPR line width and signal intensity can be attributed to changes in the amount of tin incorporated in iron nanoparticles (Figure 10). It is noticeable that the changes in the particle composition are limited, which is evidenced by the similar temperature evolution of the EPR line width of fully discharged and fully charged electrodes (Figure 8). In addition, the iron superparamagnetic particles remain sensitive whether the electrodes are fully or partially discharged. Henceforth, the EPR results agree with the existence of "spectators" iron particles which are not detected by XRD.

The proposed mechanism of interaction of nanocrystalline $FeSn_2$ with Li differs from that established for FeSn and $CoSn_2$-based electrodes.[34−36] It has been found that during the discharge both FeSn and $CoSn_2$ are directly transformed into lithium-rich Li_ySn phases and metallic Fe or Co nanoparticles, while, on charge, the "liberated" Sn atoms can react again with Fe or Co to form ferromagnetic grains of Sn−Fe alloys[36] and modified $CoSn_2$ nanocompound ($Li_yCo_zSn_2$ matrix), respectively.[33] For nanocrystalline $FeSn_2$-based electrodes studied by us, the electrochemically formed

(32) Yelsukov, E. P.; Voronina, E. V.; Konygin, G. N.; Barinov, V. A.; Godovikov, S. K.; Dorofeev, G. A.; Zagainov, A. V. *J. Magn. Magn. Mater.* **1997**, *166*, 334–348.
(33) Salado, J.; Insausti, M.; Gil de Muro, I.; Lezama, L.; Rojo, T. *J. Non-Cryst. Solids* **2008**, *354*, 5207–5209.
(34) Ionica-Bousquet, C. M.; Lippens, P. E.; Aldon, L.; Olivier-Fourcade, J.; Jumas, J. C. *Chem. Mater.* **2006**, *18*, 6442.
(35) Alcántara, R.; Ortiz, G. F.; Rodríguez, I.; Tirado, J. L. *J. Power Sources* **2009**, *189*, 309.
(36) Mao, O.; Dunlap, R. A.; Dahn, J. R. *Solid State Ionics* **1999**, *118*, 99.

superparamagnetic iron particles are preserved even after the recharge process. Their role is to prevent the particle aggregation, thus improving the electrochemical performance of $FeSn_2$-based electrodes. The different mechanism reveals the effect of nanodispersion when these materials are used as electrodes in lithium ion batteries.

Conclusions

The "one-pot" method based on polyol-solvent synthesis is suitable to produce pure nanocrystalline $FeSn_2$. These alloys deliver reversible capacities around 600 $mAhg^{-1}$ vs lithium during 20 cycles, which significantly improves previous results reported in the literature. EPR data are in agreement with the magnetic properties of nanocrystalline $FeSn_2$ with a temperature of long-range magnetic order below 140 K. The combined use of advanced spectroscopic techniques such as EPR and Mössbauer spectroscopy are helpful to understand the mechanisms of the electrochemical reactions with lithium and the improved performance of these nanodispersed materials as compared with bulk samples.

The reaction mechanism involves Li_xSn intermetallics, as shown by XRD and ^{119}Sn Mössbauer spectra. Superparamagnetic iron (and/or tin-doped iron) nanoparticles were generated during discharge and detected by both EPR and ^{57}Fe Mössbauer spectroscopy. The composition and the dimensions of the superparamagnetic particles are sensitive whether the electrodes are fully or partially discharged. The superparamagnetic iron nanoparticles are preserved even after the reverse charge process. The reversible electrochemical reaction is based on Li_xSn active species. The superparamagnetic iron (and/or tin-doped iron) nanoparticles generated during discharge avoid particle aggregation and thus improve the electrochemical performance.

Acknowledgment. J.L.T. and U.N. acknowedge the financial support from MICNN (Grant MAT2008-05880). R.A. acknowledges the financial support from MICINN (Grant CTQ2008-03192/BQU). E.Z., R.S., and M.Y. acknowledge the financial support from the National Science Fund of Bulgaria (National Centre for New Materials UNION, Contract Numbers Ch-1701/2007 and DO-02-82/2008).